An experimental investigation of evanescent wave propagation through a turning depth

Allison Lee, Julie Crockett
Department of Mechanical Engineering
Brigham Young University

Abstract

Internal waves are complex phenomena which occur uniquely in fluids which are stratified, or have varying density with respect to height. This occurs within the ocean and the atmosphere. One well known method of internal wave generation is tidal flow over oceanic bathymetry. However, in some locations, the natural frequency of the deep ocean is less than the tidal frequency and thus only evanescent waves are generated. While evanescent waves generally dissipate quickly after formation, it is been observed that if these waves travel into a stronger stratification, they can become propagating internal waves. Presented here is an experimental investigation of this internal wave generation mechanism. Specifically, internal wave energy transfer through a turning depth for a range of stratification profiles and turning depth locations is explored.

1 Introduction

Internal waves play a critical role in understanding oceanic and atmospheric dynamics. In the ocean, these waves propagate away from their generation sites and can transmit energy upward from the ocean floor when generated over topography, or downward from the ocean surface when generated by strong winds at the surface. When internal waves eventually steepen and break, mixing is induced which helps to maintain healthy oceans [1]. The same principles apply to the atmosphere where internal waves can affect both weather and climate patterns [2].

Internal waves are generated both in the ocean and the atmosphere because the density of each fluid varies with height. This is called a stratification. A strong stratification indicates large changes in density over small depths or altitudes. When a continuous, uniformly stratified fluid is disturbed (*e.g.* a collapsing thunderstorm, large schools of swimming fish, or flow over a topography *etc.*), internal waves are generated. This is similar to the ripples or waves seen when disturbing a free surface of a pond with a rock. The ocean and atmosphere are both stably stratified, allowing for the constant generation of internal waves. Peterson first recognized internal waves in 1908 and they have been a topic of much investigation since then due to their ability to transport momentum and cause mixing [3].

Propagating internal waves are only found in regions where the excitation frequency (ω) is less than the natural frequency (N). The natural frequency is described by

$$N^2 = (-g/\rho_0)(d\rho/dz) \tag{1}$$

where g is the gravitational constant, ρ_0 is a reference density for the fluid, and $d\rho/dz$ describes density as a function of depth. If the value of the excitation frequency (ω) is greater than the natural frequency (*i.e.* $\omega > N$), the bulk fluid cannot react to the excitation frequency and only evanescent waves are formed. Evanescent waves move vertically away from their generation site and the amplitude of the waves die away at an exponential rate. However, when the excitation frequency is less than the natural frequency ($\omega < N$), propagating internal waves are generated. These waves propagate away from their generation sites at an angle away from the vertical and there is little to no attenuation of the amplitude. In Figure 1, isopycnals, or

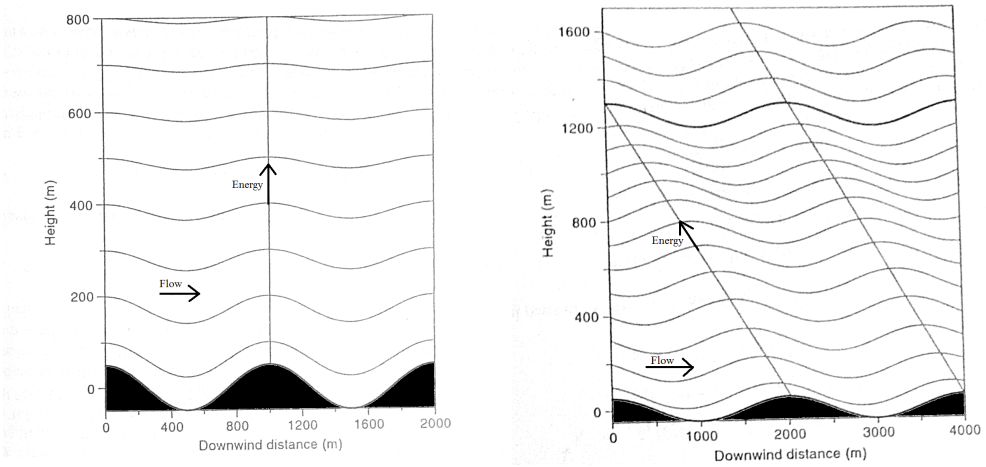

(a) Evanescent Waves

(b) Internal Waves

Figure 1: Isopycnals, or lines of constant density, are shown for evanescent waves created by flow over sinusoidal hills in (a). The amplitude of the waves die away quickly as the waves propagate vertically away from the generation location. In (b), internal waves are formed by flow over a topography and propagate away at an angle from the vertical. Adapted from Nappo [2].

lines of constant density, show the generation of both evanescent and propagating waves as fluid flows from left to right over a sinusoidal topography. Note the evanescent wave energy moves vertically upwards with a decreasing amplitude shown in Figure 1a, while the propagating waves in Figure 1b have no attenuation as they propagate at an angle from the vertical. Also, the energy of the internal wave propagates up and away to the left, while the crest and troughs of the wave seem to move to the right. The crests and troughs of internal waves are always orthogonal to the direction of energy propagation [2].

Within the ocean, one of the well known generators of internal waves is the M2 tide. As the tide oscillates over bottom topography, internal waves are formed. However, certain deep ocean locations have a natural frequency less than the M2 tidal frequency. These locations are known as evanescent regions. Usually researchers do not include these regions when estimating the amount of internal wave energy generated throughout the ocean because their rapid decay means that they have little influence on their surroundings and cause little to no oceanic mixing. However, recent research has shown the possibility of internal waves being formed out of evanescent regions [4]. Numerical simulations have shown that if evanescent wave energy reaches a turning depth, or the location where an evanescent region meets a propagating region, then that energy can become a propagating internal wave.

Tests performed in the Stratified Flow Lab have verified this prediction experimentally. Initial testing used a Gaussian-shaped peak that moved from left to right along a track. The peak was placed in an evanescent region, with a propagating region below it. These preliminary tests showed that internal waves could be formed out of an evanescent region and results are seen in Figure 2. The upper portion of the figure is an evanescent region and the peak is in the top left corner, but just out of the frame. Figure 2 is a snap shot in time as the peak moves from left to right. At a depth of approximately 0.225 m, a thin line indicates the location of the turning depth and the crests and troughs of internal waves are clearly visible in the lower portion of the image. This test indicated that internal waves could be generated experimentally from an evanescent region, but further testing was needed to understand the energy content within the propagating waves. This work will investi-

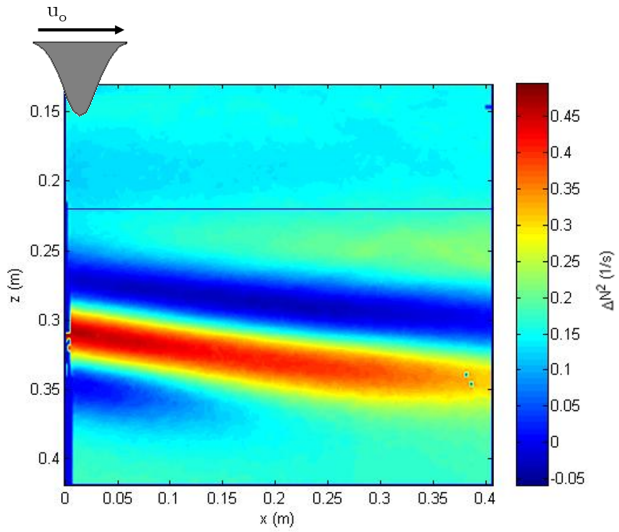

Figure 2: Initial testing showed that propagating internal waves could be generated out of an evanescent region. The Gaussian peak was pulled from left to right, and is just out side the frame shown here. The thin line at a depth of 0.225m shows the location of the turning depth. Above this line is the evanescent region. Evanescent waves are not visible in this figure, but the evidence of their existence is seen due to the presence of the propagating waves below the turning depth.

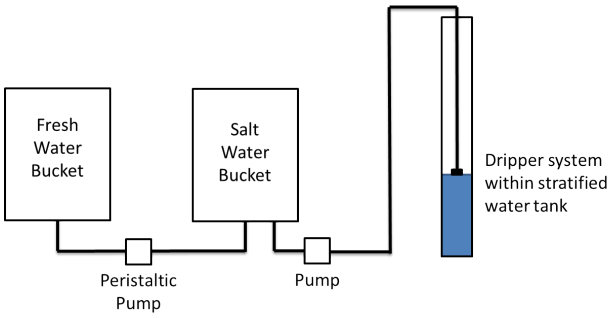

Figure 3: This setup uses a programmable peristaltic pump to control the volume flow rate of fresh water entering the salt water bucket in order to create desired stratification profiles.

gate how relative kinetic energy within internal waves is effected by the depth of the topography relative to the location of the turning depth and the stratification of the fluid.

2 Methods

2.1 Experimental Methods

To create a stratified solution in a laboratory setting, it is common to combine fresh and salty water at specific rates and densities. To generate a specific stratification, a variation of the double-bucket method as detailed by Hill [5] is used. This method takes fresh water and systemically adds it to a salt water bucket using a peristaltic pump. The salt water is then slowly added to the experimental tank to create the layered density system needed to perform experiments. Figure 3 depicts the overall setup as water transfers from the fresh water bucket to the salt water bucket and then into the actual experimental tank. The experimental tank is 2m x 1m x .15m (length, height, width), where the small width allows for the generation of two-dimensional waves while the longer length and height help prevent wave reflection from disturbing the experiment.

For all experiments considered in this work, an exponential stratification profile was generated. Exponentially changing profiles were chosen as they reflect more accurately the density changes within the ocean in certain locations [6]. A sample density profile and the accompanying natural frequency are shown in Figure 4. All experimental profiles were similar, with N values ranging from 0.5-2.0 rad/s.

To generate internal waves, a single-peak, Gaussian-shaped topography was created. The topography is oscillated along a track (as seen in Figure 5) at a constant speed. The speed is varied for different experiments and can range from 0.5-2.5 cm/s. Both the speed of the topography and the frequency of oscillation was chosen by looking at the natural frequency profile. A frequency was chosen based off of the desired distance to a turning depth. For example, using Figure 4b, if the desired turning depth was 0.3m, then the topography oscillation frequency would be set to 1 rad/s. The speed of the topography was dictated by the set frequency and the desired excursion length, or how far the topography would move in one direction.

A technique called synthetic schlieren was used to visualize and analyze the internal waves generated in each experiment [7]. Similar to the

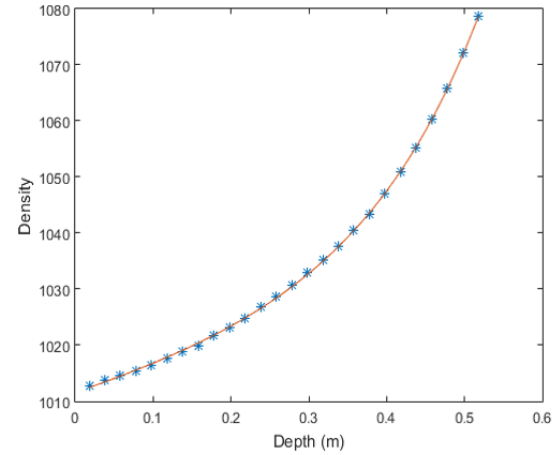

(a) Density Profile

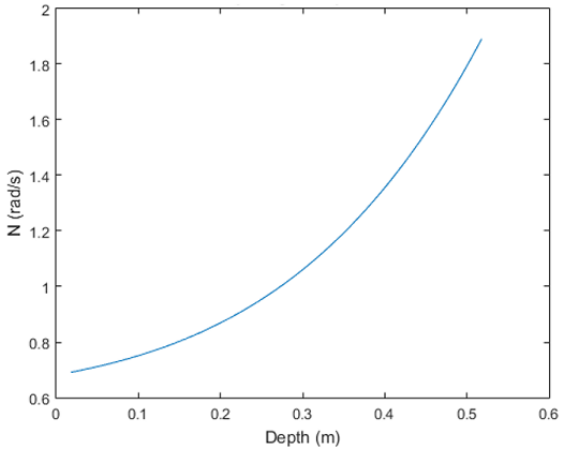

(b) Natural Frequency Profile

Figure 4: By creating an exponential density profile, the natural frequency profile was also exponential.

classical schlieren technique, this method uses the relationship between changes of index of refraction and changes in density to follow the movement of internal waves. However, instead of using a knife edge and mirrors to focus a light source, synthetic schlieren uses a dot pattern which sits directly on top of the mask shown on the right side of Figure 5. Because a change in the density of water will cause a linear change in the index of refraction, a camera can focus on the dot pattern behind the experiment and "watch" the dots move. This apparent movement is rarely visible to the naked eye, but digital image processing can identify the slight changes of the dot pattern and then correlate these to density variations[7]. A front and side view of the experimental setup, including camera placement is shown in Figure 5.

To estimate the kinetic energy within the wave, both in the evanescent and the propagating regions the software package Digiflow was used to generate values of $\Delta N_o^2(1/s)$. These indicate changes in the local stratification as waves move through the region. Wunsch and Brandt [8] found that for linear, Boussinesq waves, the kinetic energy can be estimated using

$$KE_{prop} = \frac{\omega^2 N^2}{k^2(N^2-\omega^2)+(\omega\partial_z N^2/N^2)}\left|\frac{\Delta N_o^2}{N^2}\right|^2 \tag{2}$$

where k is the horizontal wavenumber. This formula assumes a wave form for the horizontal and vertical velocities in the estimation of kinetic energy. However, the vertical velocity of evanescent waves is expressed differently as it has exponentially decaying amplitudes. The assumed vertical profiles takes on the form of

$$w(x,z,t) = \int W(k,z,\omega)\mathrm{e}^{i(kx-\omega t)}\mathrm{e}^{mz} \tag{3}$$

Where W is the Fourier coefficient of the vertical velocity, k and m are the horizontal and vertical wavenumbers, z is the vertical distance, and ω is the frequency of the wave. With this new form of the vertical velocity, the methods outlined by Wunsch and Brandt were again followed and the following equation to estimate kinetic energy within the evanescent region was derived:

$$KE_{evan} = \frac{(\omega\Delta N_0^2)^2(2-N^2/\omega^2)}{(\omega\partial_z N^2 \pm kN^2\sqrt{1-N^2/\omega^2})^2} \tag{4}$$

Equations 2 and 4 were used together to estimate how wave energy varied as it traveled from the evanescent region to the propagating region.

2.2 Analytical Methods

Along with an experimental analysis, a theoretical analysis of internal wave energy was also performed. Nappo [2] outlines a method of estimating kinetic energy of a wave moving through a turning depth, but this method assumes that the natural frequency within each region is held

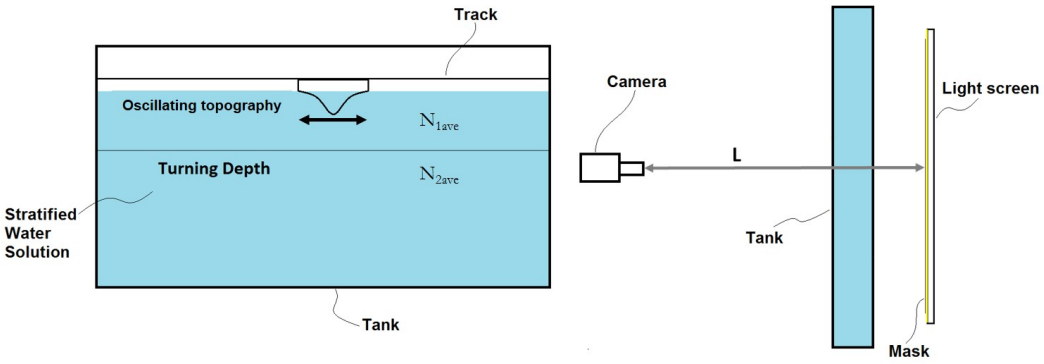

Figure 5: On the left, the topography moves left to right and generates evanescent waves in the first layer. These waves then become propagating internal waves in the second layer. The top down view on the right indicates the camera placement with the light screen and mask needed for the synthetic schlieren process behind the experiment tank.

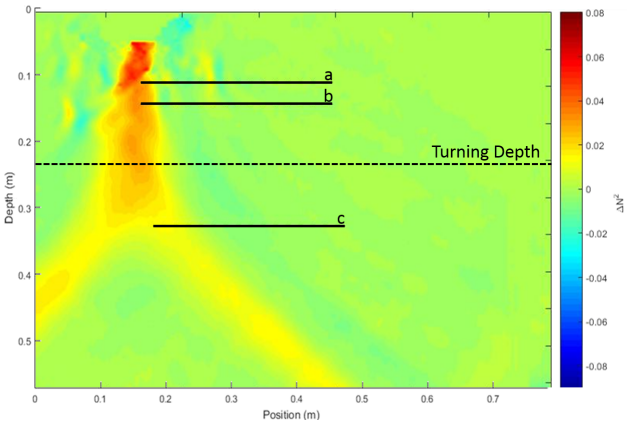

Figure 6: Estimations of kinetic energy were made both experimentally and analytically in three different locations. Two were within the evanescent region and one in the propagating region. Although not visible in this image, the topography is located right above line a.

constant. For the experiments considered here, the natural frequency varies exponentially (see Section 2.1). To account for this discrepancy, an average natural frequency was found for the evanescent (N_{1ave}) and propagating (N_{2ave}) regions, based on the density profiles of each experiment. Using this definition, values for the horizontal and vertical velocities could be found. Kinetic energy was then calculated using by $KE = 0.5(u^2 + v^2)$.

3 Results

The kinetic energy of the transitioning waves was estimated in three different locations. The first (location a) was 1 cm below the tip of the Gaussian topography, followed by a location between the topography and the turning depth (b), and finally 10 cm below the turning depth (c). The three locations (a,b,c) can be seen in Figure 6. These locations were chosen in order to see the exponential decay of evanescent wave energy as well as the energy of the propagating internal waves. The evanescent wave is seen in Figure 6 as the column of energy at approximately 0.15 m, with the two "legs" of the propagating wave below the turning depth.

Multiple scenarios were used for the experiments which were then compared to the analytical energy values. For this comparison, the energy values were scaled by a baseline value, chosen to be the energy of the evanescent wave near the topography KE_T. Thus the estimated energy values are reported as KE/KE_T. As part of the analysis, the Froude number, $Fr = \omega/N_{ave}$, and the ratio of topographical height to turning depth (H/D) were used. The Froude number represents the relative angle of propagation. Two separate Froude numbers are used, Fr_1 in the evanescent region and Fr_2 in the propagating region. All three non-dimensional numbers, Fr_1, Fr_2, and H/D, influence the energy that moves

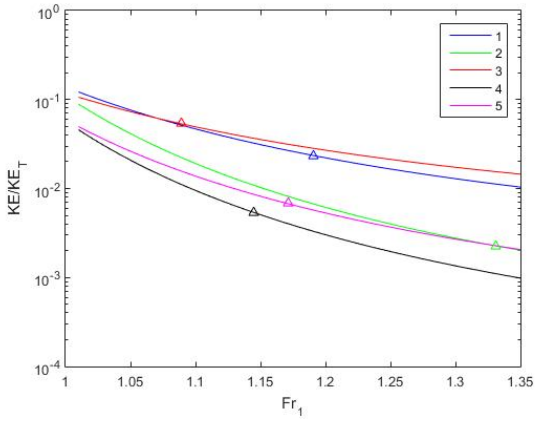

(a)

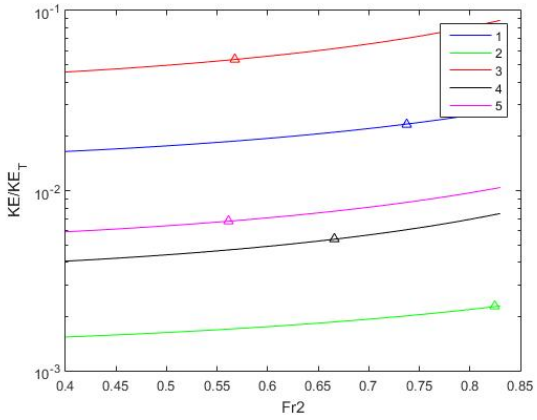

(b)

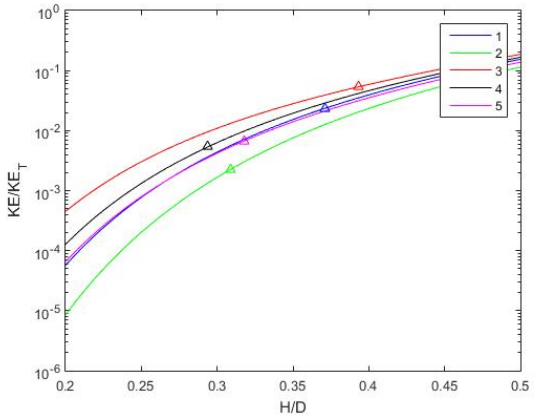

(c)

Figure 7: Each plots indicates the trend in propagating wave energy relative to Fr_1, Fr_2,and H/D. In 7a, relative kinetic energy decreases with increasing Fr_1. However, energy increases in both 7b and 7c as with increasing Fr_2 and H/D.

from the evanescent region into the propagating region.

Five different scenarios were analyzed both experimentally and analytically. Within each scenario, Fr_1, Fr_2 and H/D all varied. To understand the role of each non-dimensional number, the analytical solutions of the relative kinetic energy within the propagating region for five scenarios were plotted. Figure 7a shows the five scenarios assuming that Fr_2 and H/D were held constant while Fr_1 varied. The marker on each line corresponds to the exact analytical value that will be compared to experimental results. Figures 7b and 7c were formed similarly, with Fr_2 and H/D held constant in their respective graphs. While the five scenarios overlap in some instances, a general trend can be seen in each figure. In Figure 7a, increasing Fr_1 decreases the relative propagating kinetic energy. An increasing Fr_1 indicates an increasing excitation frequency (ω) and/or a decreasing natural frequency in the evanescent region (N_1). With N_1 decreasing, the fluid is not able to sustain the evanescent wave and the rate of exponential decay increases, causing the overall decrease in energy within the propagating region. In Figure 7b and 7c, increasing Fr_2 and H/D both cause an increase in the propagating kinetic energy. An increasing Fr_2 indicates an increase in ω and a decrease in N_2. As ω increases, the evanescent wave will originally contain more energy, allowing for a higher kinetic energy within the propagating region. When looking at an increasing H/D, the available kinetic energy increases because the distance to the turning depth is decreasing, and the amount of exponential decay also decreases.

Because each non-dimensional number varies for all five scenarios, a new combination of non-dimensional numbers was created: $(Fr_1/Fr_2)/(H/D)$. This allows a comparison of the analytical values to the experimental obtained values and is shown in Figure 8. Here relative energy values are shown in both the evanescent region and the propagating region. While the magnitudes of the analytical and experimental values are not the same, the general trends do match fairly well. The relative

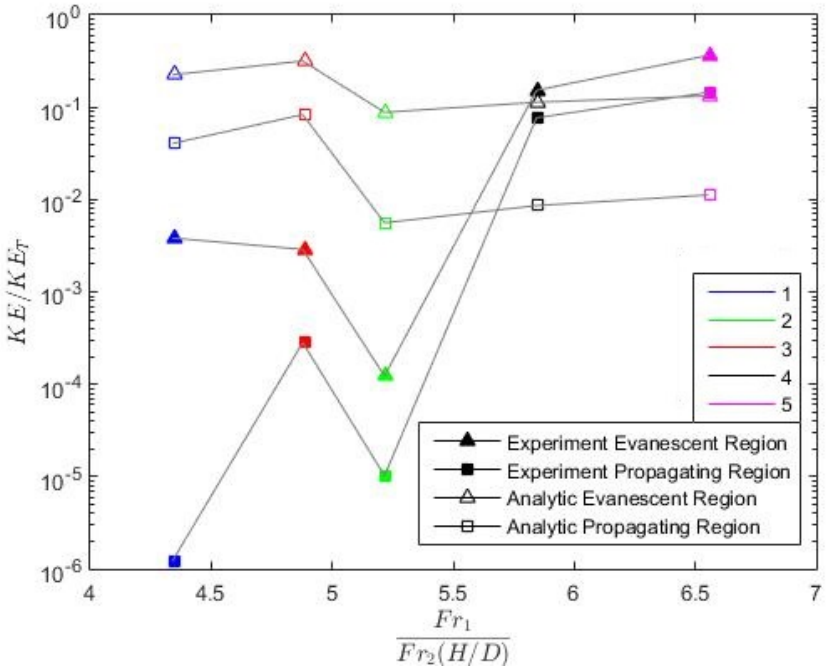

Figure 8: The experimental trends tend to follow the analytical trends. It is interesting to note that below $(Fr_1/Fr_2)/(H/D) \approx 5.25$, the analytical values overestimate the kinetic energy in the experiments, while the opposite is true above 5.25.

energy within the evanescent region is always greater than the energy within the propagating region. As the energy is decaying while traveling through the evanescent region, this trend is understandable. Also, note that the analytical values at first overestimate the experimental relative kinetic energy, but then underestimate them for higher values of $(Fr_1/Fr_2)/(H/D)$.

It is important to remember that each of the five scenario falls on a different line in Figure 7. As such, overall interpretations of increasing or decreasing energy based off of $(Fr_1/Fr_2)/(H/D)$ is not yet possible. Instead, the purpose of Figure 8 is to demonstrate that the experimental and analytical trends of increasing or decreasing energy for each value of $(Fr_1/Fr_2)/(H/D)$ are in agreement. Overall trends must be looked at from Figure 7. Based off of these analytical values, the overall energy is highest in Scenario 3, or the red line. This is most clearly seen in Figure 7b, where Scenario 3 is significantly higher than any of the other scenarios. For Scenario 3, $Fr_1 = 1.089$ which is the lowest Fr_1 among the scenarios. As seen in Figure 7a, a lower Fr_1 increases kinetic energy. It is expected that further experiments will allow for more locations to compare energy values and to create experimentally derived plots similar to those within Figure 7.

4 Conclusion

An experimental analysis of the internal wave energy and the effects of both the stratification profile (Fr) and the location of the topography (H/D) was performed. The experimental values were compared to analytical estimates at the same $(Fr_1/Fr_2)/(H/D)$ values. The general trends between the experiment and the analytical estimates are in good agreement, though the magnitudes of relative kinetic energy do not match. The analytical analysis indicates the general trends in comparing Fr_1, Fr_2 and H/D to relative kinetic energy in the propagating region. Future work includes expanding the number of scenarios to investigate both the overall trends

of Fr_1, Fr_2 and H/D and the possibility of a specific trend for $(Fr_1/Fr_2)/(H/D)$.

Acknowledgments

This research was funded in part by the Utah NASA Space Grant Consortium.

The authors are grateful to Jordan Freeman, Katie Schouten, Jeffrey Carruth, Austin Maxwell, Jake Lessie, Kelsie Cummings, Mitchell Gehlbach, and Taylor Stewart for their assistance in performing experiments.

References

[1] B. R. Sutherland, *Internal Gravity Waves*. Cambridge, United Kingdom: Cambridge University Press, 2010.

[2] C. J. Nappo, *An introduction to atmospheric gravity waves*. San Diego, California: Academic Press, 2002.

[3] C. Garret and W. Munk, "Internal waves in the ocean," *Annual Review of Fluid Mechanics*, pp. 339–369, 1979.

[4] M. S. Paoletti, M. Drake, and H. L. Swinney, "Internal tide generation in nonuniformly stratified deep oceans," *Journal of Geophysical Research: Oceans*, vol. 119, no. 3, pp. 1943–1956, 2014.

[5] D. F. Hill, "General density gradients in general domains: the two-tank method revisited," *Experiments in Fluids*, vol. 32, no. 4, 2002.

[6] B. King, M. Stone, H. P. Zhang, T. Gerkema, M. Marder, R. B. Scott, and H. L. Swinney, "Buoyancy frequency profiles and internal semidiurnal tide turning depths in the oceans," *Journal of Geophysical Research: Oceans*, vol. 117, no. C4, 2012.

[7] S. B. Dalziel, G. O. Hughes, and B. R. Sutherland, "Whole-field density measurements by 'synthetic schlieren'," *Experiments in Fluids*, vol. 28, no. 4, pp. 322–335, 04/01 2000.

[8] S. Wunsch and A. Brandt, "Laboratory experiments on internal wave interactions with a pycnocline," *Expts. in Fluids*, vol. 53, pp. 1663–1679, 2012.